# P1E.2 PRELIMINARY ANALYSIS OF MESOSCALE CONVECTIVE SYSTEMS TRANSITIONING OFF THE WEST AFRICAN COAST DURING NASA AFRICAN MONSOON MULTIDISCIPLINARY ANALYSIS (NAMMA)

Bradley W. Klotz[1] and Paul A. Kucera[1, 2]
[1] University of North Dakota, Grand Forks, North Dakota*
[2] National Center for Atmospheric Research/Research Applications Laboratory, Boulder, Colorado†

## 1. INTRODUCTION

Tropical storms and hurricanes in the Atlantic Ocean are significant components of the energy transport from the lower latitudes to the higher latitudes of the globe. However, these storms can take their toll on the people and places that lie within their path. Because of the possible effect on human life, it is important to understand the generation and formation of these systems in an effort to improve the public awareness of these events.

One way to increase public awareness is to improve upon the forecast methods of tropical cyclones. Studying the locations where the systems originate is a great place to begin when trying to improve upon the prediction methods. For most landfalling and non-landfalling cases in the Atlantic Basin, tropical storms and hurricanes form as a direct result of African Easterly Waves (AEW) and Mesoscale Convective Systems (MCS) moving off the West African coast during the African Monsoon season (Burpee, 1972; Thorncroft and Hodges 2001). Over half of the AEW that move off the coast are found to produce tropical cyclones (Frank, 1970; Burpee, 1972). The Sahel region of Africa, which is bounded by the Sahara Desert to the north and tropical regions to the south, is where the AEW originate and propagate. The dynamics behind AEW formation are reliant on several factors. Two of these factors are the African Easterly Jet (AEJ) and the low-level flow, both of which are instrumental to the formation and strengthening of the AEW in the Sahel (Cook, 1999; Diedhiou et al., 1999). The Intertropical Convergence Zone (ITCZ) has been found to have a large impact on the formation of the AEJ and thus the AEW and subsequent precipitation (Janicot, 1992a). For more information on the flow patterns over the Sahel and their relation to precipitation and AEW formation, see papers by Kanamitsu et al. (1972), Chen (1980), Lamb (1983), Chen and van Loon (1987), Fontaine and Janicot (1995), Cook (1999), and Diedhiou et. al (1999).

As the synoptic flow of the AEJ and low-level monsoon flow act to produce AEW, the AEW also act to produce precipitation and MCS formation in the Western Sahel. The maximum amount of precipitation across the Sahel occurs during the months of August and September, which corresponds with a peak in the number of AEW (Grist, 2002; Nicholson and Grist, 2003). A majority of this rainfall is produced by squall line type MCS's (Rowell and Milford, 1993; Fink and Reiner, 2003). The dynamics and orientation of AEW are determinants of MCS generation on a synoptic level, but Convective Available Potential Energy (CAPE) and low-level wind shear are important for ensuring squall line type formation (Parker et al., 2005; Mohr and Thorncroft, 2006). Diurnal variation can have a profound impact on the strengths of the MCS. The diurnal variation of precipitation over land and ocean environments in the tropics is well documented by Aspliden et al. (1976) and Nesbitt and Zipser (2003). It was found that a majority of the squall line production over land occurred between the hours of 12 and 18 UTC.

A question that still remains is what is the relationship between AEW and squall line type MCS development? In many cases, there have been strong similarities to the timing between the two, especially with rainfall amount (Reed, 1977; Diedhiou et. al (1999); Fink and Reiner, 2003). However, some cases have shown the opposite to be true (Bolton, 1984; Duvel, 1990). Studying the structure of precipitation from the MCS that are produced by AEW is necessary to find a relationship between these interactions and with tropical cyclone formation. This study

* *Corresponding author address:* Bradley W. Klotz, Department of Atmospheric Sciences, Clifford Hall 400, 4149 University Avenue Stop 9006, Grand Forks, ND 58202-9006; email: brad.klotz@und.nodak.edu

† *Corresponding author address:* Paul A. Kucera, NCAR/Research Applications Laboratory, P.O. Box 3000, Boulder, CO 80307-3000; e-mail: pkucera@ucar.edu

attempts to find such a relationship between the structure and environment of these MCS in the hopes of ultimately being used to improve forecasting methods for tropical storm development.

## 2. DATA

The NAMMA datasets are very extensive due to the large array of instruments that were used during the project. The NASA Polarimetric Doppler Radar (NPOL), radiosonde data from Kaswara, Senegal and Dakar, Senegal, NCEP Reanalysis data of 700 and 500 mb geopotential heights, and European Meteorological Satellite (EUMETSAT) infrared images were all used to determine characteristics of the MCS that occurred during the field project.

The NPOL radar was deployed in Kaswara, Senegal, which is approximately 40 km southeast of Dakar. NPOL was operational from 1415 UTC 21 August, 2006 through 1200 UTC 30 September, 2006. The exact location of NPOL was 14.656 °N, 17.098 °W. NPOL had a maximum range of 270 km while in surveillance scan mode. Volumetric scans had a maximum range of 150 km. NPOL is a dual polarized radar. The following observables were available from NPOL data: radar reflectivity, Doppler velocity, spectrum width, differential reflectivity, specific differential reflectivity, and correlation coefficient. These data from a total of 19 MCS events were observed by NPOL during the project.

The radiosonde data collected from Kaswara are very sporadic due to the criteria of launches. In most cases, radiosondes were launched if precipitation was within the detectable range of NPOL. For a more consistent dataset, radiosondes from Dakar, Senegal are also used even though they were not part of the NAMMA instrumentation.

Fields from the NCEP Reanalysis and EUMETSAT datasets were analyzed during the entire length of the NAMMA campaign. However, a more focused analysis of these fields was performed based on the timing of the MCS cases. For the period of four to six hours prior to MCS detection by NPOL, geopotential height fields at 700 and 500 mb were used to observe locations of AEW trough axes. EUMETSAT images were used to find the location of AEW generation. All images of NCEP Reanalysis data were obtained from the NOAA-ESRL Physical Sciences Division, Boulder, Colorado from their Web site at http://www.cdc.noaa.gov/.

## 3. METHODS

Choosing the MCS events to study was based on reports from the National Hurricane Center in Florida. The objective was to find all of the named storms that formed during the time of NPOL operations and to use the Tropical Cyclone Reports to determine when the AEWs associated with these cyclones moved off the coast. There were three named storms during NPOL operations (Florence, Gordon, and Helene). There were four AEW associated with these cyclones because two AEW were involved in the formation of Hurricane Florence. The Tropical Cyclone Reports are available online through the National Hurricane Center archive at http://www.nhc.noaa.gov/2006atlan.shtml. The four MCS events associated with these named storms will be considered as Type I systems. Four of the other MCS cases were chosen based on the similarities of organization and structure to the Type I systems. The four that did not result in tropical cyclone formation will be referred to as Type II systems. Table 1 shows the eight MCS cases that are used.

Table 1. Selected events for analysis. Listed are the case number as it appears in the NPOL operations log, system type (I or II), the date, and the time span in universal time. All dates are from 2006.

| Case # | Type | Date | Time UTC |
|---|---|---|---|
| 5 | I | 8/29 | 11 - 14 |
| 6 | I | 8/31 | 06 - 13 |
| 7 | I | 9/01 - 9/02 | 22 - 04 |
| 10 | II | 9/07 - 9/08 | 16 - 10 |
| 11 | I | 9/11 | 08 - 15 |
| 12 | II | 9/13 - 9/14 | 18 - 08 |
| 15 | II | 9/22 | 12 - 18 |
| 18 | II | 9/28 | 00 - 06 |

From the events in Table 1, vertical cross-sections of radar reflectivity, Doppler velocity and spectrum width were created. The purpose of these cross-sections was to compare the echo-top heights, strongest reflectivity and strongest reflectivity heights of Type I and II systems. Also, Contoured Frequency by Altitude Diagrams (CFAD) were created from the NPOL data. CFADs for Type I and Type II systems were created along with CFADs for oceanic and terrestrial surfaces. For more information related to CFADs, consult Yuter and Houze (1995).

The methods of choosing the radiosonde data were dependent upon the cases in Table 1. The Dakar, Senegal radiosondes were launched every 12 hours. The observations that were closest to the start of an event were chosen, but the data had to be recorded before the detection of precipitation by NPOL. Kaswara radiosonde observations were chosen in a similar manner, but some of the data were collected while NPOL was observing precipitation. Soundings were produced using RAOB ®. From the soundings, dewpoint temperature depression, relative humidity, and vertical wind shear were determined for each case.

NCEP Reanalysis and EUMETSAT data were chosen similarly to that of the radiosonde data. EUMETSAT images were combined with NCEP Reanalysis 700 mb geopotential heights to determine the origins of the AEW associated with each case. The main purpose of the Reanalysis data is to provide a synoptic overview of the area and to determine the location of the AEW trough.

## 4. RESULTS AND DISCUSSION

The systems listed in Table 1 are presented in Fig. 1. There were a large number of cross-sections created, so the images shown are the times that were the most intense throughout each event. It turns out that the Type I systems were much better organized and more intense in terms of radar reflectivity.

The results from the various analysis methods proved to be quite revealing about the structure and environment associated with the MCS presented in Table 1. When comparing the echo-top heights between the system types, which are shown in Fig. 2, the Type II systems have a larger total number and a larger probability of having higher echo-top heights than the Type I systems. The heights are divided into four bins for each system type for the echo-top heights. For the echo-top heights, there is over 10% greater probability for the Type II systems to have echo-top heights above 14 km and nearly 5% greater for heights of 8 to 11 km. However, the opposite is true for the Type I systems in that there is over 11% greater probability of having echo-top heights from 5 to 8 km. Keep in mind that the Type II systems occurred in the late afternoon or evening, which is a time that has been observed to produce the deepest convection (e.g., Nesbitt and Zipser, 2003).

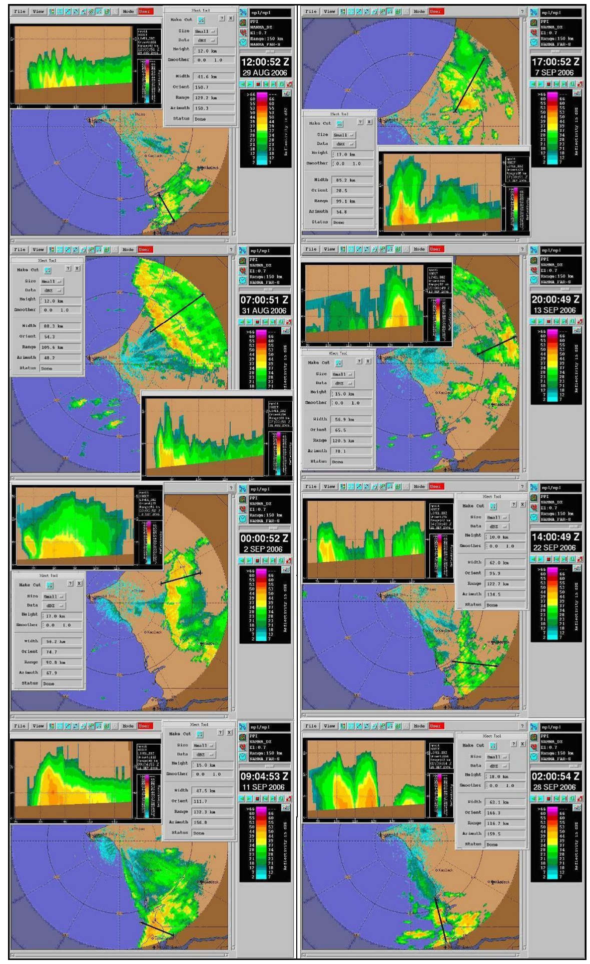

Figure 1. NPOL cross-sections of peak intensity for the MCS events listed in Table 1. The left column contains the Type I systems beginning with Case 5. The right column contains the Type II systems starting with Case 10. The bold, black line indicates the cross-section line.

The strongest reflectivity and height of the strongest reflectivity have opposite trends when compared to the trends of echo-top heights. Figure 3 contains the frequency of occurrence for the strongest reflectivity and heights. The strongest reflectivity values for this study rarely exceeded 55 dBZ. Therefore, reflectivity was categorized into the following bins: < 35 dBZ, 35-40 dBZ, 40-45 dBZ, 45-50 dBZ, and ≥ 50 dBZ. The height bins were divided into < 3 km, 3-4 km, 4-5 km, and > 5 km. From the probabilities calculated from the occurrences at each height and bin, there is an 11% greater probability for Type II to have maximum reflectivity values between 45-50 dBZ from 3-4 km and a 5% greater probability for reflectivity values above 50 dBZ at the same height range. Type I systems have a 14% greater chance of having reflectivity values of 45-50 dBZ from 4-5 km and a 9.5% greater chance of 40-45 dBZ at heights above 5 km.

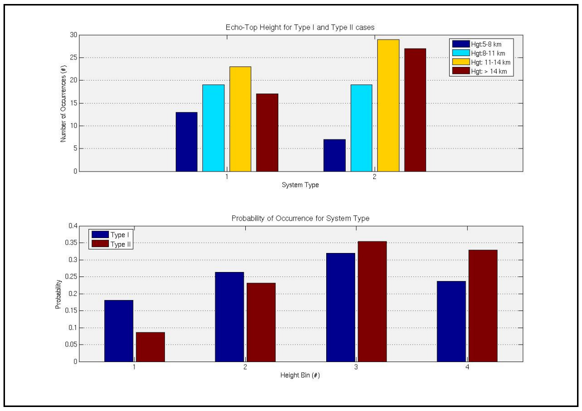


Figure 2. Frequency of occurrence (top) and probability (lower right) for echo-top heights.

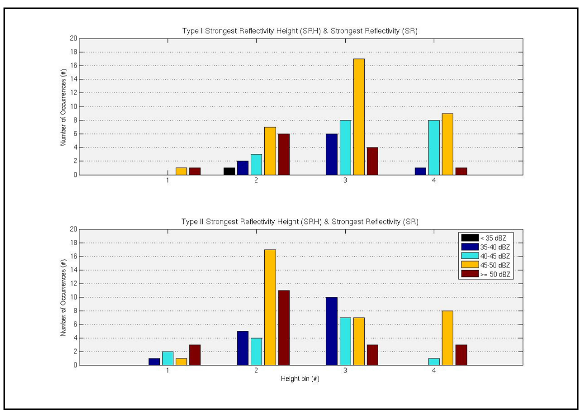


Figure 3: Frequency of occurrence for strongest reflectivity and heights for Type I (top) and Type II (bottom) systems. Each group represents a height bin and each color code represents a reflectivity bin.

CFAD analysis also provides distinguishable differences between the two system types. CFADs were created once every hour for the duration of each event. Overall CFADs were created for each event and each system type. These overall CFADs are shown in Fig. 4. When comparing the CFADs for each overall event between the two system types, there is a clear difference in the frequency of heights and reflectivity values. Trying to detect a shift in the percentages either to higher or lower reflectivity values or to higher or lower heights between the two system types is the goal with these CFADs. The Type I systems have somewhat of a shift of the 4-6% range to a value of about 2.5 dBZ lower as compared with the Type II systems, but these percentages do not extend to the lower heights as observed with the Type II systems. With occurrences greater than 6%, which would be considered the peak percentage range, the Type I systems have a less broad range of reflectivity and also do not extend to as low of heights as the Type II systems. The narrower range and less vertical extent of percentage indicate that the nature of these two systems is somewhat different. The Type II cases have more stratiform precipitation throughout the event, which causes a broadening in the peak and extent of the percentages. With less stratiform precipitation occurring in the Type I events, the range and extent of the peak is more concentrated and has less variation.

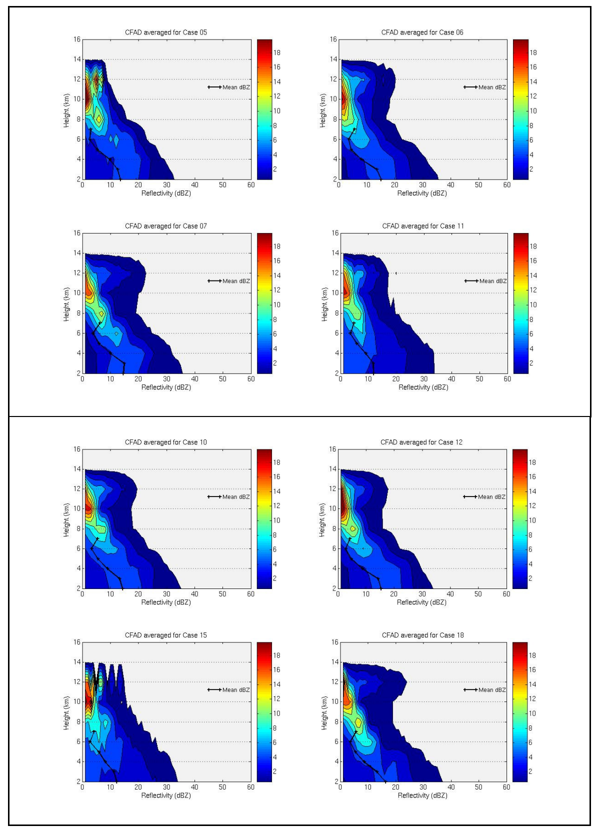

Figure 4. The overall CFADs for each case are shown for the Type I systems (top four) and Type II systems (bottom four). Each case is listed in chronological order with the top right beginning with Case 5 and Case 10 for the respective system types.

Moisture and instability indices are important aspects to consider in an examination of convection. Understanding the effect the environment will have on generation of convection is important for this study. The indices used to characterize the convection include: CAPE, dewpoint temperature depression, relative humidity, and vertical wind shear. It has been shown that the Type I systems are much more organized and tend to be more intense than the Type II cases. Looking only at CAPE, it would be hard to justify any kind of differences between the two types. For both sets, there was no definite threshold of CAPE that separated Type I and Type II from each other. The soundings from Kaswara showed that CAPE could have a threshold at near 3000 $Jkg^{-1}$, but the Dakar soundings did not produce similar results. The CAPE values were still higher with the Type I cases as overall, but there was no set threshold with the Dakar soundings. However, there was a noticeable difference in the dewpoint temperature depressions between system type. Table 2 shows the average dewpoint depression from 550 to 400 mb for each case. Figure 5 shows the Kaswara temperature, dewpoint temperature, and dewpoint temperature depression for each case. The Kaswara radiosonde launches ended on September 15, so there were no data for Case 15 or 18. From Table 2, it is seen that the middle levels of the troposphere are significantly drier for Type II systems. Drier air at these levels implies more dry air entrainment, which is detrimental to convective production (Rogers and Yau, 1989).

Table 2. Average dewpoint temperature depressions ($T_d$) from 550 to 400 mb for Kaswara and Dakar, Senegal are shown. All Temperatures are in °C.

| Site | Date Time | $T_d$ Depr | Date Time | $T_d$ Depr |
|---|---|---|---|---|
| KAS | 06/08/29 1740 | -19.37 | 06/09/06 2201 | -20.68 |
| KAS | 06/08/31 0000 | -8.05 | 06/09/13 1738 | -19.35 |
| KAS | 06/09/01 1702 | -7.93 | | |
| KAS | 06/09/11 0549 | -13.00 | | |
| KAS | **Total** | -12.09 | | -20.02 |
| DAK | 06/08/29 0000 | -10.91 | 06/09/07 1200 | -20.03 |
| DAK | 06/08/31 0000 | -14.37 | 06/09/13 1200 | -26.72 |
| DAK | 06/09/01 1200 | -5.23 | 06/09/22 1200 | -26.37 |
| DAK | 06/09/11 0000 | -24.00 | 06/09/28 0000 | -8.21 |
| DAK | **Total** | -13.63 | | -20.33 |

Vertical wind shear also plays an important role in the development of squall line type MCS production. Low-level vertical wind shear has been found in many cases to be a determinant of squall line production (Weisman, 1993; Weisman and Rotunno, 2004). Figure 6 shows the wind shear for each case at Kaswara. All cases had somewhat significant values of vertical wind shear at low levels (e.g. below 3 km), but a distinct difference in the wind shear at the 550 to 300 mb pressure levels exists between the two system types. Significant directional and speed shear is present with the Type II cases especially above 400 mb. The Type I cases did have some shear at the higher levels, but the shear was greater on average for the Type II events. Stronger wind shear aloft also contributes to a lack of convective development, which is seen in the analysis of the NPOL radar reflectivity data.

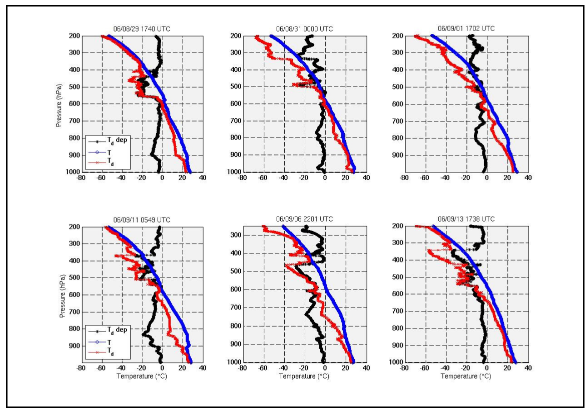

Figure 5. Temperature (blue), dewpoint temperature (red), and dewpoint temperature depression (black) for each case at Kaswara. The pressure scale is plotted from 1000 to 200 mb. The top right panel in Case 5 and the others follow in order of case number with system type. The bottom two on the right are for Cases 10 and 12, respectively.

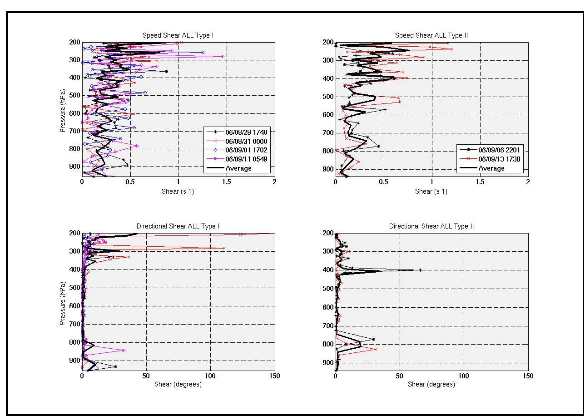


Figure 6. Vertical speed (top) and directional (bottom) wind shear for Kaswara. All Type I events are in the left panels with average as a bold black line. The Type II events are in the right 2 panels.

## 5. CONCLUSIONS

The data that were gathered during NAMMA were used to determine structural characteristics of MCS squall line events as well as determine some environmental parameters of the area near the West African coast. The NPOL cross-sections of radar reflectivity showed that even though the echo-top heights were higher for the Type II cases, the strongest reflectivity values and associated heights were consistently higher and more intense for the Type I systems. The CFADs also showed that the nature of the precipitation that occurred was proportioned differently. With more stratiform precipitation signatures appearing in the CFADs for the Type II events, a difference in the ranges of reflectivity and height were found. Type II cases had broader ranges of peak frequency in terms of reflectivity values.

The soundings that were produced provided some key information about the environment associated with systems that do not produce tropical cyclones. With both the Kaswara and Dakar, Senegal sites, a distinguishable difference between the two system types was found in the dewpoint temperature depressions from 550 to 400 mb. Drier air associated with the Type II cases leads to less developed and organized convection, which is what was observed by NPOL. The vertical wind shear differences were not as well defined but were still present. The significant wind shear at low-levels was found for both system types as a requirement for squall line development, but greater values of directional shear and speed shear were found above 400 mb with the Type II events.

These results provide a starting point for continuing studies related to this topic. From what has been gathered with this research, a preliminary idea of structural, organizational, and environmental characteristics associated with squall lines that produce tropical cyclones has been produced. Continuing the study using Doppler radar observations of squall lines along with continued radiosonde launches during the period of the African monsoon is necessary for validating and expanding upon the results that were produced through this study. Possibly a conceptual model of tropical storm formation could be created from some of the ideas presented.

*Acknowledgements: This research was conducted under NASA grant: NNX06AC73G. Thanks to Dr. Paul Kucera, Dr. Mark Askelson, and Dr. David Delene at the University of North Dakota for assistance throughout the work. Thanks to Mr. Christopher Theisen at the University of North Dakota for assistance with some of the NPOL data.*

### REFERENCES

Aspliden, C. I., Y. Tourre, and J. B. Sabine, 1976: Some Climatological Aspects of West African Disturbance Lines during GATE. *Mon. Wea. Rev.*, **104**, 1029-1035.

Bolton, D., 1984: Generation and Propagation of African Squall Lines. *Quart. J. Roy. Meteor. Soc.*, **110**, 695-721.

Burpee, R.W.,1972: The Origin and Structure of Easterly Waves in the Lower Troposphere of North Africa. *J. Atmos. Sci.*, **29**, 77-90.

Chen, T. C., and H. van Loon, 1987: Interannual Variation of the Tropical Easterly Jet. *Mon. Wea. Rev.*, **115**, 1739-1759.

——, 1980: On the Energy Exchange Between the Divergent and Rotational Components of Atmospheric Flow over the Tropics and Subtropics at 200 mb during Two Northern Summers. *Mon. Wea. Rev.*, **108**, 896-912.

Cook, K. H., 1999: Generation of the African Easterly Jet and Its Role in Determining West African Precipitation. *J. Climate*, **12**, 1165-1184.

Diedhiou, A., S. Janicot, A. Viltard, P. de Felice, and H. Laurent, 1999: Easterly Wave Regimes and Associated Convection over West Africa and Tropical Atlantic: Results from the NCEP?NCAR and ECMWF Reanalyses. *Clim. Dynam.*, **15**, 795-822.

Duvel, J. P., 1990: Convection over Tropical Africa and the Atlantic Ocean during Northern Summer. Part II: Modulation by Easterly Waves. *Mon. Wea. Rev.*, **118**, 1855-1868.

Fink, A. H., and A. Reiner, 2003: Spatio-temporal Variability of the Relation between African Easterly Waves and West African Squall Lines in 1998 and 1999. *J. Geophys. Res.*, **108**, 4332, doi:10.1029/2002JD002816.

Fontaine, B., S. Janicot, and V. Moron, 1995: Rainfall Anomaly Patterns and Wind Field Signals over West Africa in August (1958-1989). *J. Climate*, **8**, 1503-1510.

Frank, N. L., 1970: Atlantic Tropical Systems of 1969. *Mon. Wea. Rev.*, **98**, 307-314.

Grist, J. P., 2002: Easterly Waves over Africa. Part I: The Seasonal Cycle and Contrasts between Wet and Dry Years. *Mon. Wea. Rev.*, **130**, 197-211.

Janicot, S., 1992a: Spatiotemporal Variability of West African Rainfall. Part I: Regionalizations and Typings. *J. Climate*, **5**, 489-497.

Kanamitsu, M., T. N. Krishnamurti, and C. Depradine, 1972: On Scale Interactions in the Tropics during Northern Summer. *J. Atmos. Sci.*, **29**, 698-706.

Lamb, P. J., 1983: West African Water Vapor Variations Between Recent Contrasting Subsaharan Rainy Seasons. *Tellus, Ser. A*, **35**, 198-212.

Thorncroft, C. D., and K. Hodges, 2001: African Easterly Wave Variability and Its Relationship to Atlantic Tropical Cyclone Activity. *J. Climate*, **14**, 1166-1179.

Nicholson, S. E. and J. P. Grist, 2003: The Seasonal Evolution of the Atmospheric Circulation over West Africa. *J. Climate*, **16**, 1013-1030.

Mohr, K. I., and C. D. Thorncroft, 2006: Intense Convective Systems in West Africa and Their Relationship to the African Easterly Jet. *Quart. J. Roy. Meteor. Soc.*, **132**, 163-176.

Nesbitt, S. W. and E. J. Zipser, 2003: The Diurnal Cycle of Rainfall and Convective Intensity according to Three Years of TRMM Measurements. *J. Climate*, **16**, 1456-1475.

Parker, D. J., C. D. Thorncroft, R. R. Burton, and A. Diongue-Niang, 2005: Analysis of the African Easterly Jet, Using Aircraft Observations from the JET2000 Experiment. *Quart. J. Roy. Met. Soc.*, **131**, 1461-1482.

Reed, R. J., D. C. Norquist, and E. E. Recker, 1977: The Structure and Properties of African Wave Disturbances as Observed during Phase III of GATE. *Mon. Weath. Rev.*, **105**, 317-333.

Rogers, R. R., and M. K. Yau, 1989: *A Short Course in Cloud Physics, Third Edition*, Butterwoth Heinemann Publications. 290 pp.

Rowell, D. P., and J. R. Milford, 1993: On the Generation of African Squall Lines. *J. Climate*, **6**, 1181-1193.

Weisman, M. L., and R. Rotunno, 2004: “A Theory for Strong, Long-Lived Squall Lines” Revisited. *J. Atmos. Sci.*, **61**, 361-382.

———, 1993: The Genesis of Severe, Long-Lived Bow Echoes. *J. Atmos. Sci.*, **50**, 645-670.

Yuter, S. E., and R. A. Houze, 1995: Three-Dimensional Kinematic and Microphysical Evolution of Florida Cumulonimbus. Part II: Frequency Distributions of Vertical Velocity, Reflectivity, and Differential Reflectivity. *Mon. Wea. Rev.*, **123**, 1941-1963.